Fossil Record 29 (2) 2026, 599–610 | DOI 10.3897/fr.29.193112

PENSOFT

MUSEUM FÜR NATURKUNDE BERLIN

# A case of an expansile lesion in a caudal vertebra of *Medusaceratops lokii*

Donghao Wang[1,2], Lida Xing[3,4], Bruce M. Rothschild[5], Chunlei Du[4], Kexiang Wen[4], Jin Lin[4], Mengling Kang[4], Jiayin Su[6]

1 *Mineral Resources Survey Division, Harbin Center for Natural Resources Comprehensive Survey, China Geological Survey, Harbin 150039, Heilongjiang, China*
2 *Observation and Research Station of Earth Critical Zone in Black Soil, Ministry of Natural Resources, Harbin 150086, China*
3 *State Key Laboratory of Geomicrobiology and Environmental Changes, School of Earth Sciences and Resources, Frontiers Science Center for Deep-time Digital Earth, China University of Geosciences, Beijing, 100083, China*
4 *Grandview Museum of Natural Science, Guangzhou, 510620, China*
5 *Department of Medicine, Indiana University Health, Muncie, IN 47303, USA*
6 *Department of Plastic Surgery, Fengcheng Hospital, Shanghai, 201411, China*

https://zoobank.org/40D48356-BEF2-416D-ADFE-4DF6407AF284

Corresponding author: Lida Xing (xinglida@gmail.com)

Academic editor: Florian Witzmann ♦ **Received** 27 March 2026 ♦ **Accepted** 24 July 2026 ♦ **Published** 6 August 2026

## Abstract

This study presents the first documented case of chronic osteomyelitis with a draining sinus tract in the centrosaurine ceratopsid *Medusaceratops lokii*, based on a pathological seventh caudal vertebra from the Upper Cretaceous Judith River Formation of Montana. Integrated macroscopic and computed tomography analyses revealed pathognomonic features of chronic osteomyelitis secondary to trauma, including extensive hyperostosis with "cauliflower-shaped" bone overgrowths, moth-eaten osteolysis, sclerosis, a definitive sinus tract, and occult fractures associated with the destruction of the bilateral transverse processes. The development of a substantial involucrum confirms prolonged post-traumatic survival, attesting to robust immunological resilience in ceratopsid dinosaurs. A review of the 81 reported cases of dinosaurian infection indicates that osteomyelitis represents the predominant lesion type and that the great majority of cases are post-traumatic. Bone infection therefore appears to have been seeded principally through traumatic breaches rather than arising chiefly via non-traumatic routes, and the anatomical distribution of infectious lesions also differs among the major clades.

## Key Words

Ceratopsidae, computed tomography, Judith River Formation, osteomyelitis, paleopathology

## Introduction

Paleopathology, an interdisciplinary field bridging paleontology and medicine, occupies an increasingly pivotal position within vertebrate paleontology. Researchers have identified evidence of antemortem pathologies in fossilized skeletal remains (e.g., Xing et al. 2024), eggs (e.g., Jackson et al. 2004), integument (e.g., Rothschild and DePalma 2013), and even ichnofossils (e.g., Herrera-Castillo et al. 2022). Non-avian dinosaurs, in particular, have been the subject of a growing number of case reports. These pathologies are diverse, encompassing fractures (e.g., Xing et al. 2009), infections (e.g., Rothschild et al. 2023), neoplasms (e.g., Ekhtiari et al. 2020), ankylosis secondary to arthritis (e.g., Xing et al. 2015), hyperostosis (e.g., Foth et al. 2015), dental disease (e.g., Xing et al. 2013), and congenital and developmental anomalies (Baiano et al. 2024), among others.

Among these conditions, cases of infection are documented relatively frequently. Infection is defined as the

Copyright: This is an open access article distributed under the terms of the CCO Public Domain Dedication.

invasion of a host organism by pathogenic microorganisms—such as bacteria, viruses, fungi, or parasites—and the subsequent elicitation of an immunological cascade (Bennett et al. 2019). This process typically results in tissue damage and induces an inflammatory response; associated clinical manifestations may include erythema, pyrexia, pain, and functional impairment (Murphy and Weaver 2016). Pathogens may enter the host via various routes, including the respiratory tract, gastrointestinal tract, or compromised integument (Cohen et al. 2016). In pathological contexts, infections in the fossil record are often discernible through osseous lesions. For instance, pathological hyperostosis (Tanke and Rothschild 2002) or erosive features visible in computed tomography (CT) imagery (Xing et al. 2018) may imply past infection, typically manifesting as abnormal cortical thickening or irregular surface bone overgrowths (Tanke and Rothschild 2002). The analysis of such lesions facilitates inferences regarding dinosaurian behavior, environmental stressors, and the evolution of the immune system (Rothschild et al. 2023). As of June 2026, 81 dinosaurian cases involving infection have been scientifically reported, comprising 20 in Cerapoda, nine in Thyreophora, 13 in Sauropodomorpha, and 39 in Theropoda (Suppl. material 1).

Ceratopsia represents a significant clade of Cretaceous herbivorous dinosaurs; their distinctive cranial frills and facial horns likely functioned in defense, as well as in courtship and intraspecific competition (Padian and Horner 2011). Existing research indicates that various ceratopsians exhibited a spectrum of pathologies. For example, a fibular fracture has been documented in *Psittacosaurus lujiatunensis* (Hedrick et al. 2016), while *Psittacosaurus* sp. has exhibited signs of fibular necrosis (Lü et al. 2007). Abnormal bone resorption was observed on the supraorbital horn of *Centrosaurus apertus* (Ryan et al. 2001), alongside a rare case of osteosarcoma (Ekhtiari et al. 2020). Fenestrae on the squamosals of *Diabloceratops eatoni* and *Pentaceratops* sp., potentially attributable to trauma, have also been identified (Tanke and Farke 2006; Kirkland and DeBlieux 2010). *Pachyrhinosaurus lakustai* exhibited fractures in the metacarpals (Vice 2020). Furthermore, the nasal boss of *P. perotorum* demonstrated pathological changes consistent with fractures and osteomyelitis, while traces of trauma and infection were identified on the caudal vertebrae (Fiorillo and Tykoski 2023). Although Tanke and Rothschild (2010) documented several caudal vertebral pathologies in ceratopsian dinosaurs from Alberta, none of the reported lesions is comparable to the expansile osteomyelitic lesion described in the present study. Punctures and fractures in the horns and frills of *Triceratops* sp. are likely associated with combat behavior (Nabavizadeh 2023), whereas *Vagaceratops irvinensis* displays signs of degenerative articular changes in the cervical vertebrae and metacarpals (Holmes et al. 2001; Sampson et al. 2010).

*Medusaceratops lokii* was originally referred to as the basal centrosaurine *Albertaceratops nesmoi* (Ryan 2007). Subsequently, Ryan et al. (2010) reassigned the material to Chasmosaurinae based on the two most complete parietals, establishing the new genus and species via an analysis of specimens distinguished by the presence of only three epiparietals on either side of the midline. Longrich (2013) later returned the taxon to Centrosaurinae, arguing that the number of epiparietals is variable within Chasmosaurinae and that the morphology of the parietosquamosal junction bears greater similarity to that observed in Centrosaurinae. Chiba et al. (2018) incorporated new fossil material alongside previously described specimens into a numerical cladistic analysis, the results of which supported Longrich's (2013) conclusion. The available evidence indicates that *Medusaceratops lokii* is currently regarded as a distinct taxon from *Albertaceratops nesmoi*, representing the prevailing scientific consensus.

## Materials and methods

The specimen described herein was recovered from light-colored sandstones of the Upper Cretaceous Judith River Formation near Joplin (Havre), Montana, USA. It is currently housed at the Grandview Museum of Natural Science in Guangzhou, China, under the accession number HS0385 (HS = Mandarin Pinyin abbreviation for "fossil"; Fig. 1). Specimen HS0385 derives from a nearly complete skeleton, although individual elements are incomplete or damaged, most notably portions of the skull; of the caudal series, only the seventh caudal vertebra is pathological.

The morphological characteristics of HS0385 conform to the diagnosis of *Medusaceratops lokii* established by Chiba et al. (2018). Specifically, it is identified as a centrosaurine ceratopsid possessing five epiparietals on the posterolateral parietal ramus, arranged medially to laterally as follows: epiparietal 1 (ep 1) is small and slightly procurved; epiparietal 2 (ep 2) is a comparatively large, broad-based pachyostotic projection that curves strongly anterolaterally; epiparietal 3 (ep 3) forms a smaller pachyostotic process with an anterolateral curvature similar to that of ep 2; and epiparietals 4 and 5 (ep 4 and ep 5) are unmodified, manifesting as small, triangular ossifications. The pathology of HS0385 is present in the seventh caudal vertebra.

CT imagery was acquired using an ANATOM P419 scanner (120 kV, 350 mA, 280 mAs), designed and manufactured by Shenzhen Anke High-tech Co., Ltd., Shenzhen, China. The external surface of the specimen was scanned using an Artec Spider structured-light scanner, and the acquired data were processed and reconstructed in Artec Studio.

A dataset comprising 81 cases of dinosaurian infection was compiled (Suppl. material 1), and statistical analyses were performed in PAST v5.3 (Hammer et al. 2001) to test for associations between taxon or ecological niche and both trauma type and the anatomical location of infection. For 2 × 2 contingency tables, Fisher's exact test was used, whereas larger contingency tables were

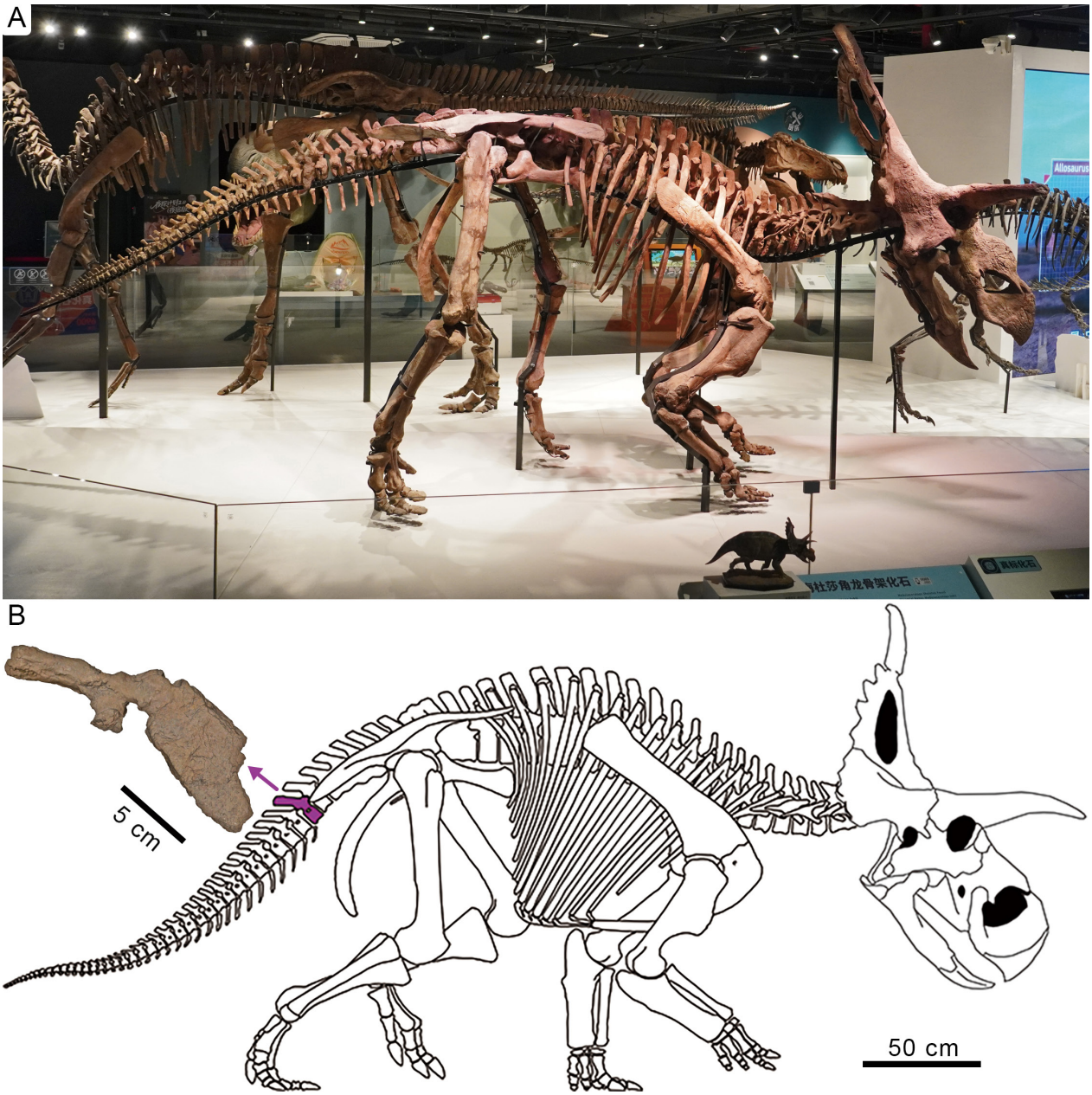


**Figure 1.** Mounted skeleton (**A**) and line drawing of the skeleton (**B**) of HS0385. The purple bone represents the pathological seventh caudal vertebra.

analyzed using the chi-square test in combination with Monte Carlo permutation tests (999 replicates). A similar approach was employed by Baiano et al. (2024) to investigate the relationship between taxonomic affiliation and ecological niche. Effect sizes are reported as Cramér's *V*, and the significance threshold was set at $\alpha = 0.05$.

# Results

## Description

The seventh caudal vertebra exhibits gross expansile pathological deformation. The lateral surfaces and posterior articular surface of the centrum are covered by reactive bone exhibiting a honeycomb-like texture. The anterior and posterior articular facets of the centrum remain discernible; the anterior facet measures 50.1 mm in width and 68.8 mm in height, while the posterior facet measures 55.8 mm in width and 61.7 mm in height (Fig. 2). The remaining caudal vertebrae are slightly smaller than the corresponding elements in *Styracosaurus albertensis* (Holmes and Ryan 2013), whereas the seventh caudal vertebra is distinctly smaller than both its counterpart in *S. albertensis* and the immediately adjacent sixth and eighth caudal vertebrae.

The vertebra is characterized by the conspicuous absence of the bilateral transverse processes (Fig. 2). A partial remnant of the left transverse process is preserved (Fig. 2D$_1$), measuring 27.6 mm in maximum width, 40.8 mm in

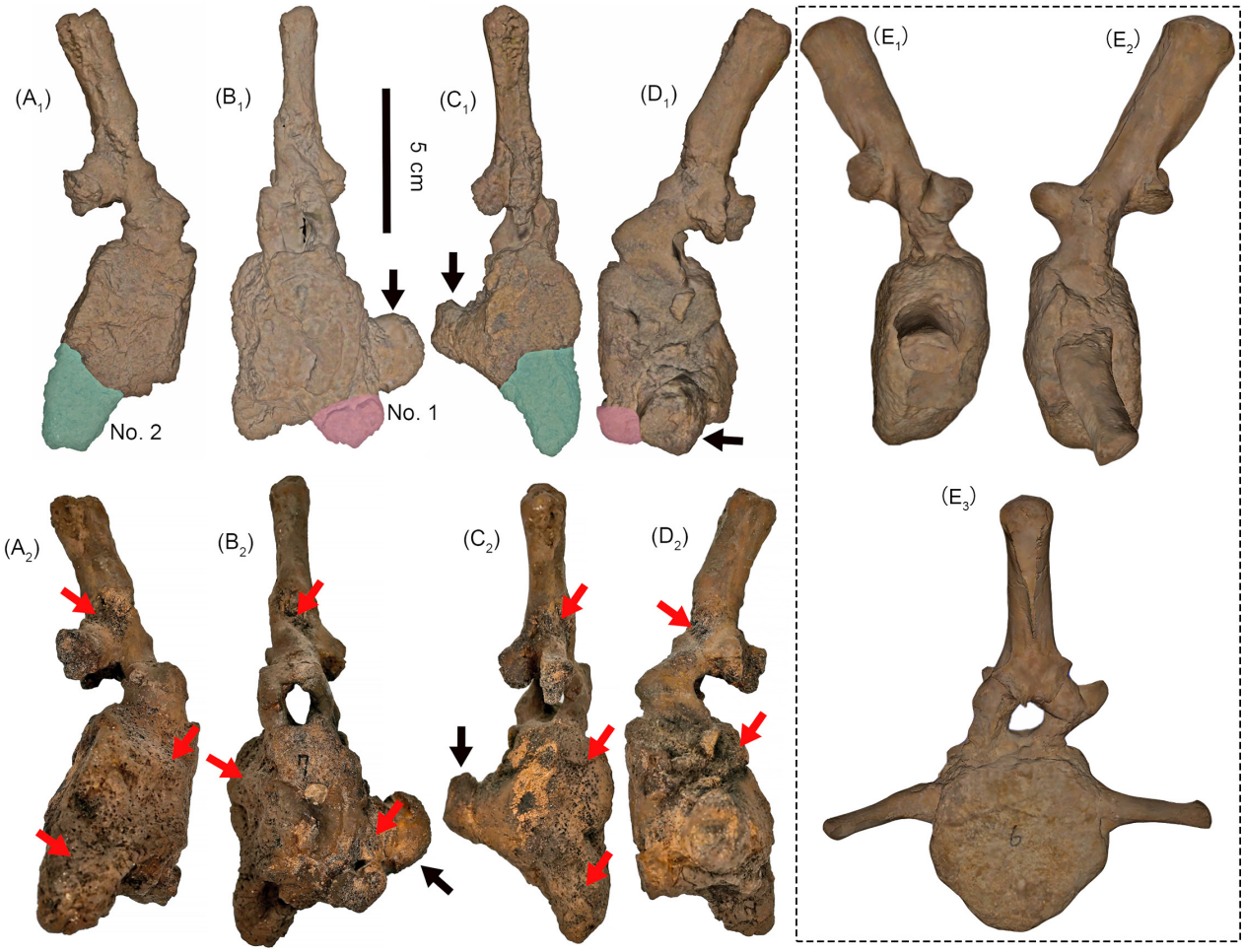


**Figure 2.** The seventh caudal vertebra of HS0385: **$A_1$.** Right lateral view of the 3D reconstruction; **$B_1$.** Cranial view of the 3D reconstruction; **$C_1$.** Caudal view of the 3D reconstruction; **$D_1$.** Left lateral view of the 3D reconstruction; **$A_2$.** Right lateral view; **$B_2$.** Cranial view; **$C_2$.** Caudal view; **$D_2$.** Left lateral view of the actual fossil. Light pink represents bone overgrowth No. 1, and teal represents bone overgrowth No. 2; red arrows indicate the honeycomb-like texture; black arrows indicate the remnant of the left transverse process. The sixth caudal vertebra of HS0385: **$E_1$.** Right lateral view of the 3D reconstruction; **$E_2$.** Left lateral view of the 3D reconstruction; and **$E_3$.** Caudal view of the 3D reconstruction. The 3D reconstructions (**$A_1$–$D_1$, $E_{1–3}$**) are surface models generated from data acquired using the Artec Spider scanner; **$A_2$–$D_2$** are photographs of the corresponding views.

height, and 35.4 mm in length. Its cranial cortical surface remains relatively smooth and continuous, whereas the remaining surfaces exhibit a honeycomb texture. This structure represents the vestige of a fractured transverse process, with evident hyperostosis at its terminus. The right side lacks the distinct fracture trace observed on the left (Fig. 2$A_1$); however, slightly dorsal to the relative position of the left process, there is an elliptical hyperostotic feature with raised margins and a depressed center, characterized by rough cortical bone. The dimensions and relative position of this elliptical trace are consistent with those of a transverse process; consequently, this area is interpreted as the vestige of the right transverse process.

The centrum exhibits multiple exophytic bone overgrowths, two of which exceed 20 mm in width. Bone overgrowth No. 1 connects to the ventral surface of the centrum via a broad craniocaudal pedicle, extending cranially to form a plane roughly parallel to the anterior articular facet. This surface is honeycombed, and the bone overgrowth displays an irregular, "cauliflower-shaped" morphology. The lateral cortical margin of bone overgrowth No. 1 is relatively smooth, whereas other areas lack a continuous, smooth cortex. It measures 28.6 mm in maximum width and 41.5 mm in length, with the pedicle constituting the majority of its length. Bone overgrowth No. 2 is "beak-shaped," measuring 38.1 mm in maximum width, 57.3 mm in height, and 44.1 mm in length. The ventral expansion of bone overgrowth No. 2 appears to overlie bone overgrowth No. 1. Additionally, smaller bone overgrowths with surface textures similar to those of bone overgrowths No. 1 and No. 2 are present on the right lateral aspect of the centrum.

The prezygapophyseal articular facets exhibit pathological abnormalities. The left facet displays expansile changes with a rough, honeycombed surface. The postzygapophyseal facets show similar anomalies with varying degrees of expansion; the changes are more pronounced

on the right than on the left. The left caudoventral margin is honeycombed, while the entire surface of the right facet exhibits this texture. The neural spine adjacent to the postzygapophyses displays comparable expansile changes over a vertical range of 24.6 mm, featuring discontinuous cortical bone and a honeycombed surface.

## Imaging manifestations

CT imaging reveals "moth-eaten" osteolytic destruction within both the bone overgrowths and the vertebral body (Fig. 3). All bone overgrowths demonstrate continuity with the cortical and cancellous bone of the centrum. The two primary bone overgrowths are particularly distinct in the CT imagery. High-density regions are evident at the lateral margins of the bone overgrowths and the centrum; density decreases heterogeneously toward the interior, forming focal osteolytic lesions. The periosteum of the non-pathological portions of the centrum is difficult to distinguish accurately. Localized regions of homogeneous density are present within the centrum. Distinct cavities and fissures are observable within the bone overgrowths and the internal structure of the normal bone, surrounded by marked, homogeneous high-density zones (sclerosis).

A sinus tract is identified at the margin of the right-sided region of the centrum; in coronal sections, it constitutes a clearly visible channel draining to the exterior of the bone (Fig. 3). The prezygapophyses, postzygapophyses, and adjacent neural spine form heterogeneous regions

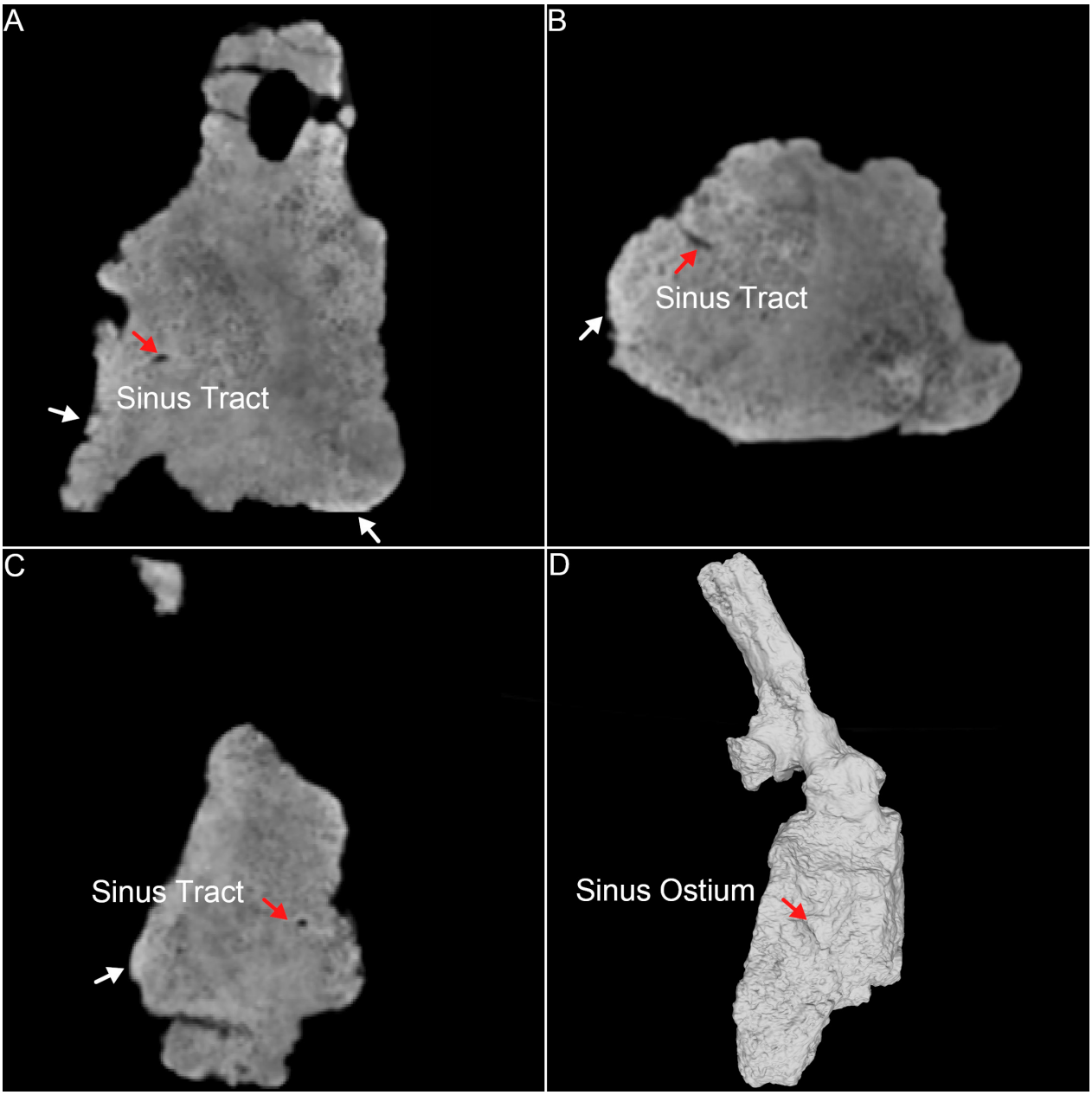


**Figure 3.** CT imaging of the seventh caudal vertebra of HS0385: **A.** Axial section; **B.** Coronal section; **C.** Sagittal section; and **D.** 3D right lateral view. Red arrows indicate the sinus tract; white arrows indicate sclerosis.

of mixed high and low density. Occult fracture lines are identifiable in the axial and bilateral sagittal sections (Fig. 4). The fracture line is penetrating in the cranial and right sections but does not extend deeply into the centrum; in the left sagittal section, only a minimal portion of the fracture line is visible.

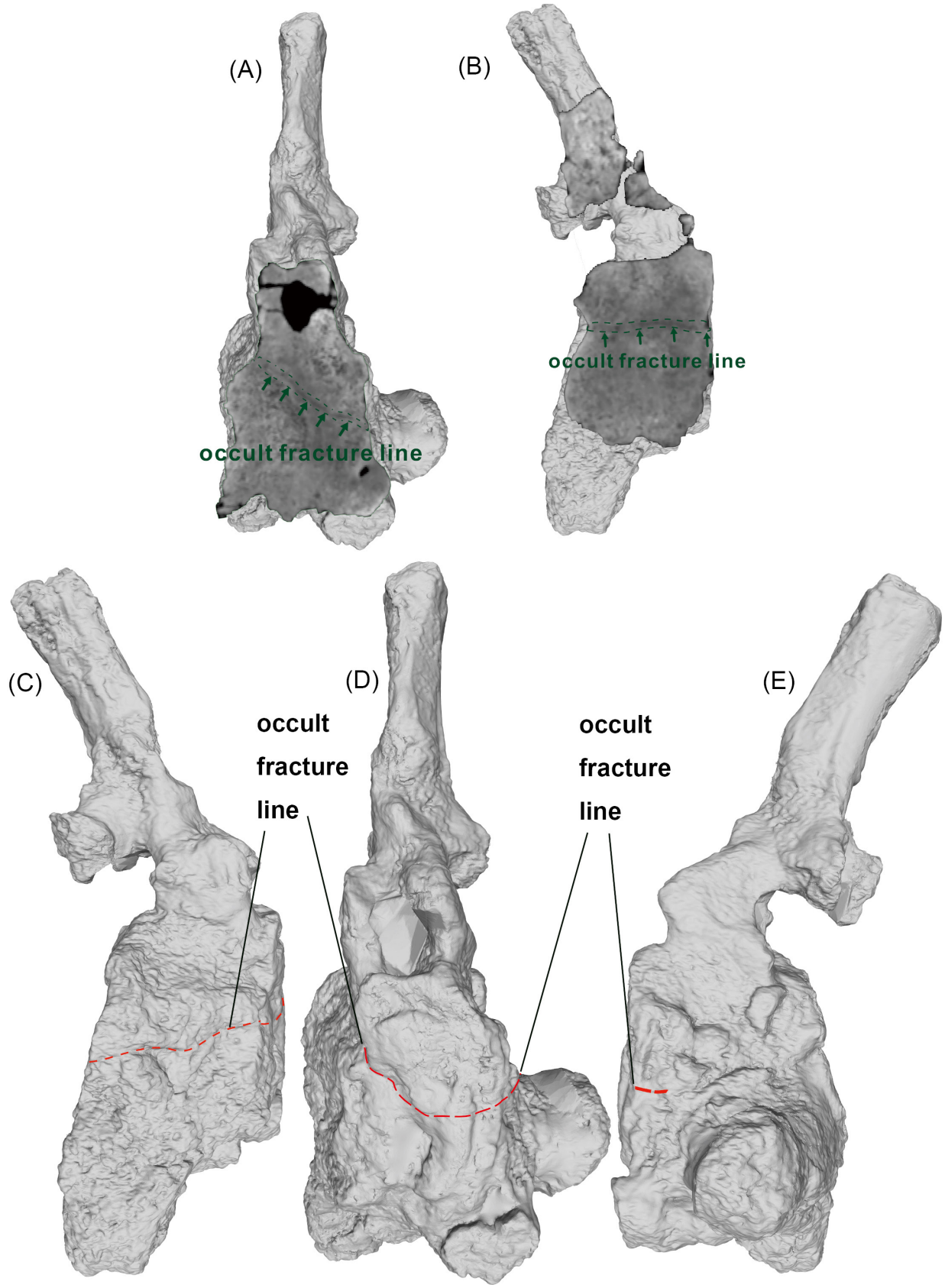


**Figure 4.** Location of the occult fracture line in the seventh caudal vertebra of HS0385 in axial (**A**) and right sagittal (**B**) CT sections and in 3D right lateral (**C**), cranial (**D**), and left lateral (**E**) views.

# Discussion

Synthesizing the morphological alterations and CT manifestations of the seventh caudal vertebra, the pathological characteristics may be summarized as follows: (1) Extensive expansile hyperostosis and honeycomb-like surface changes: The vertebra exhibits gross expansile abnormalities. In the affected regions, the cortical bone is discontinuous, and a rough, honeycomb-like texture is widely distributed across the surface of the element, indicating an active periosteal reaction or bone remodeling secondary to chronic inflammation. (2) Prominent heteromorphic bone overgrowths: Significant bone overgrowths have developed on the ventral aspect of the centrum, displaying "cauliflower-shaped" or "beak-like" morphologies with substantial volume (both maximum length and height exceed 20 mm). CT imaging confirms that these bone overgrowths are continuous with the cortical and cancellous bone of the centrum and contain internal cavities and fissures surrounded by sclerotic high-density zones. (3) "Moth-eaten" osteolytic destruction and mixed-density manifestations: The lesion area displays highly heterogeneous density, characterized by a "high-density margin, low-density center" pattern accompanied by focal osteolytic lesions. (4) Traces of old trauma and occult fractures: The right transverse process is absent and replaced by a hyperostotic stump or elliptical osseous trace, consistent with healed, historic trauma following fracture of the process. Furthermore, CT scans reveal occult fracture lines in the transverse and right sagittal sections; these lines partially penetrate but do not extend deeply into the vertebral interior, further confirming that the vertebra suffered external trauma that resulted in incomplete healing or malunion. (5) Sinus tract identification: A definitive sinus tract is identified at the right margin of the centrum. In the coronal section, this manifests as a channel penetrating the cortical bone and connecting the internal pathological focus with the external environment. (6) Given that the remaining caudal vertebrae are comparable in size to those of adult individuals, the relatively small centrum of the seventh caudal vertebra may indicate that the lesion developed during ontogeny and subsequently influenced the growth of this element.

## Diagnosis and behavioral implications

Expansile osseous lesions are typically differentially diagnosed as follows: (1) infection-induced expansile lesions, such as osteomyelitis (Meyer et al. 2011), tuberculosis (Greenspan and Remagen 1998), and parasitic infection (Resnick 2002; Nielsen and Rosenberg 2017); (2) metabolic diseases, such as Paget's disease of bone (Witzmann et al. 2011); (3) benign lesions, including osteomas (Fechner and Mills 1993), ossifying fibromas (Dunfee et al. 2005), bone cysts (Wang et al. 2003), enchondromas (Meyer et al. 2011), chondroblastoma (Kong and Cai 2021), and giant cell tumors (Meyer et al. 2011); (4) malignant lesions, such as osteosarcoma (Kong and Cai 2021), chondrosarcoma (Kong and Cai 2021), fibrosarcoma (Kong and Cai 2021), chordoma (Kong and Cai 2021), and myeloma (Kong and Cai 2021); and (5) arthropathies, such as spondyloarthropathy (de Souza Barbosa et al. 2018).

Given the irregular morphology of the bone overgrowths and the rough, discontinuous cortex observed in this specimen, bone cysts, fibrous dysplasia, enchondromas, chondroblastoma, giant cell tumors, and the majority of benign tumors can be excluded (Kong and Cai 2021). In cases of malignant neoplasms and infectious lesions, persistent pathological stimulation of the periosteum induces abnormal proliferation, resulting in the formation of irregular bone overgrowths (Kong and Cai 2021). The rapid formation of these bone overgrowths often outpaces cortical formation or produces a cortex lacking normal structural integrity, leading to a discontinuous surface. CT imagery reveals clear bone overgrowth boundaries with high-density marginal layering, indicative of hyperostosis and a periosteal reaction typical of chronic inflammation; this permits the exclusion of metastatic tumors, osteosarcoma, and myeloma (Kong and Cai 2021). Under the prolonged influence of chronic inflammation or stress fractures, the periosteum is continually stimulated to generate new bone, which subsequently calcifies and hardens, forming layered high-density structures. This stratification typically results from repeated periosteal or osseous proliferation. In this specimen, such features are observed not only in the bone overgrowths and centrum but also in the neural arch. The "moth-eaten" osteolytic erosion observed in CT scans is predominantly associated with malignant tumors and chronic infections, allowing for the exclusion of parasites and Paget's disease of bone (Kong and Cai 2021). Arthropathies such as spondyloarthropathy (de Souza Barbosa et al. 2018) typically involve the intervertebral articulations and produce enthesiophytes (syndesmophytes) on multiple adjacent vertebrae. By contrast, in HS0385, bony overgrowth is confined to the seventh caudal vertebra, making spondyloarthropathy an unlikely diagnosis. Malignant cells or infectious pathogens destroy the bone matrix via the release of proteases and lytic enzymes, causing local osteolysis. These agents invade trabecular bone, forming small, irregular lytic defects. Chronic inflammatory lesions, such as chronic osteomyelitis, are accompanied by the release of local immune cells; the inflammatory cytokines produced by these cells also stimulate osteolysis, resulting in irregular bone defects. The neural arch of this specimen exhibits identical manifestations (Kong and Cai 2021). The sinus tract is a specific pathological feature of chronic osteomyelitis. Its formation mechanism involves intramedullary hypertension caused by pyogenic infection within the medullary cavity, forcing fibriscess material and necrotic tissue outward as they erode the cortical bone and form a drainage channel to relieve pressure (Huchzermeyer and Cooper 2000). In paleopathological and radiographic diagnosis, the presence of a sinus tract not only confirms the connection between a deep infectious focus and the external

environment but also serves as a critical functional criterion for distinguishing deep osteomyelitis from simple superficial periostitis (Resnick 2002). In conclusion, based on the fractured bilateral transverse processes and the evidence of historic trauma and occult fractures, the diagnosis is chronic osteomyelitis secondary to trauma.

The severe post-traumatic chronic osteomyelitis present in this specimen provides key clues to the behavior of cerapodans. The seventh caudal vertebra is located at the tail base, a primary target zone for theropod predation and a common point of impact in cerapodan intraspecific combat (e.g., flank-butting or tail-swinging) (Siviero et al. 2020; Cruzado-Caballero et al. 2021). The destruction of the bilateral transverse processes and traces of open trauma imply that this individual survived an episode of extreme physical confrontation. Notably, despite suffering a deep infection accompanied by a draining sinus, the presence of a massive involucrum and extensive internal sclerosis confirms that the individual survived for a considerable period following the severe injury. Baiano et al. (2024) conducted a statistical survey of theropod paleopathologies and analyzed the resulting dataset. Their results indicated a non-random anatomical distribution of lesions, with the axial skeleton showing the highest frequency of pathological involvement across all pathology types combined rather than for infectious cases specifically. This may reflect the recurrent exposure of the axial skeleton to mechanical stress, intraspecific interactions, or predation-related injuries during life. Although HS0385 is not a theropod, the occurrence of chronic osteomyelitis in a caudal vertebra is broadly consistent with the pattern reported by Baiano et al. (2024).

The seventh caudal vertebra of HS0385 is situated in the anterior portion of the tail, a region of functional importance for normal activity (Persons and Currie 2011). Following the initial trauma, prolonged tail movement may have generated additional stress fractures, thereby increasing the likelihood of wound opening and facilitating progression to severe infection. The seventh caudal vertebra is situated within the origin of the *M. caudofemoralis longus*, the principal femoral retractor muscle responsible for hindlimb retraction during locomotion (Persons and Currie 2011). Consequently, this vertebra would have experienced sustained mechanical loading throughout locomotion, thereby increasing the likelihood and severity of mechanical damage. The inability of the animal to reduce the mechanical load on the injured caudal vertebra may have perpetuated callus disruption and promoted microbial invasion of cancellous bone, a recognized pathway for contiguous-spread osteomyelitis (Resnick 2002; Lew and Waldvogel 2004). The large-scale gregarious behavior documented in centrosaurines (Ryan et al. 2001; Eberth and Getty 2005) may also have increased the exposure of injured individuals to environmental pathogens through substrate contamination associated with herd living.

Stress fractures are relatively common across Dinosauria (e.g., Rothschild and Tanke 1992; Rothschild and Molnar 2005). Among ceratopsians, they are most frequently documented in *Pachyrhinosaurus*, *Styracosaurus*, and *Triceratops*, predominantly affecting the proximal phalanges of pedal digits III and IV (Rothschild 1988; Rothschild and Tanke 1992). In sauropods, both the manus and pes represent common sites of stress-related injury (Rothschild and Molnar 2005; Rothschild et al. 2023). Among theropods, stress fractures have been reported in *Allosaurus*, *Ceratosaurus*, *Tarbosaurus*, and dromaeosaurids (Rothschild et al. 2001; Rothschild and Tanke 2005; Anné et al. 2015), with additional occurrences noted in other tyrannosaurids (Rothschild et al. 2023). Notably, stress fractures in the *Allosaurus* pes occur at approximately equal frequencies across digits II–IV, which does not support a running-induced etiology; if running were the primary cause, a higher incidence would be expected in digit III. Rothschild et al. (2001) instead proposed that these injuries may have been associated with predatory behavior.

Theropods may have mitigated loading on an injured hind limb through compensatory use of the contralateral pes. The trackway described by Herrera-Castillo et al. (2022), in which the left pes shows digital abnormalities, whereas the right footprints indicate greater loading, is consistent with such compensatory behavior. Cruzado-Caballero et al. (2021) likewise argued that pathological conditions do not necessarily result directly in severe locomotor impairment. Several *Allosaurus* specimens further show that pedal infections could be effectively contained as localized involucra rather than progressing to diffuse osteomyelitis (Hanna 2002; Foth et al. 2015). Together with the comparatively high metabolic rates inferred for theropods (Grady et al. 2014), this has been interpreted as potentially reflecting a more vigorous innate immune response.

## Infection statistics

Infectious cases are relatively common in dinosaurian paleopathology; as of June 2026, 81 such cases have been compiled (Suppl. material 1). Osteomyelitis represents the predominant category in the infection dataset, accounting for 84.0% of cases (68/81), whereas the remaining cases include septic arthritis, parasitism, respiratory infection, and other less frequent conditions. This predominance is consistent with osteomyelitis being the infectious lesion most readily recognized in fossil bone or, alternatively, the type most likely to be preserved in the fossil record. The great majority of cases are post-traumatic infections that preserve evidence of antecedent trauma, accounting for 59.0% of the dataset (48/81), whereas non-traumatic cases comprise only 21.0% (17/81). Among the post-traumatic cases, the recorded specific injury mechanisms include fractures

other than stress fractures (28 cases), open or puncture wounds (14 cases), cranial impact injuries (four cases), and limb amputation (one case). The marked predominance of post-traumatic cases indicates that, within the diagnosable dinosaurian fossil record, bone infection was seeded principally through traumatic breaches of the integument or skeleton, consistent with contiguous-spread osteomyelitis (Resnick 2002; Lew and Waldvogel 2004), rather than arising chiefly from hematogenous or other non-traumatic routes. These data describe the composition of reported cases and may therefore be subject to overrepresentation. Because the sample includes only infected individuals, post-traumatic osteomyelitis with associated fractures or wounds is more readily recognized than primary hematogenous osteomyelitis, and approximately one-quarter of cases have an indeterminate trauma mechanism, these proportions are likely to be influenced by diagnostic and taphonomic biases.

The anatomical distribution of infectious lesions also differs among the major clades (Fig. 5). Axial-skeletal involvement predominates in thyreophorans and sauropodomorphs; theropod lesions are more evenly distributed across the cranial, axial, and appendicular regions and girdle; and cerapodan lesions occur mainly in the cranial and axial skeleton. The association between clade and anatomical region is statistically detectable ($\chi^2$ = 25, df = 9, $P$ = 0.004; Cramér's $V$ = 0.32). Caudal lesions are significantly overrepresented in Sauropodomorpha relative to other clades (Fisher's exact test, $P$ = 0.004; Cramér's $V$ = 0.35), a pattern that may be related to the functional and behavioral importance of the sauropod tail. However, these associations should be regarded as descriptive and hypothesis-generating rather than as confirmatory evidence of causal relationships.

## Conclusion

This study presents the first documented case of chronic osteomyelitis with a draining sinus tract in *Medusaceratops lokii*, diagnosed from a pathological seventh caudal vertebra (HS0385) recovered from the Upper Cretaceous Judith River Formation of Montana. Integrated macroscopic and CT analyses reveal pathognomonic features of chronic osteomyelitis secondary to trauma, including moth-eaten osteolysis, extensive involucrum formation, and occult fractures associated with the destruction of the bilateral transverse processes. The presence of a definitive sinus tract—a hallmark of deep osteomyelitis—together with the massive involucrum and internal sclerosis, confirms that the individual survived for a prolonged period following the initial traumatic insult, attesting to robust immunological resilience in ceratopsid dinosaurs.

A review of the 81 reported cases of dinosaurian infection further indicates that osteomyelitis is the predominant lesion type and that the great majority of cases are post-traumatic. The anatomical distribution of infectious lesions also differs among clades: in theropods, lesions are concentrated mainly in the cranium and the axial and appendicular skeletons; in thyreophorans and sauropodomorphs, they are concentrated in the axial skeleton; and in cerapodans, lesions occur predominantly in the cranial and axial skeleton.

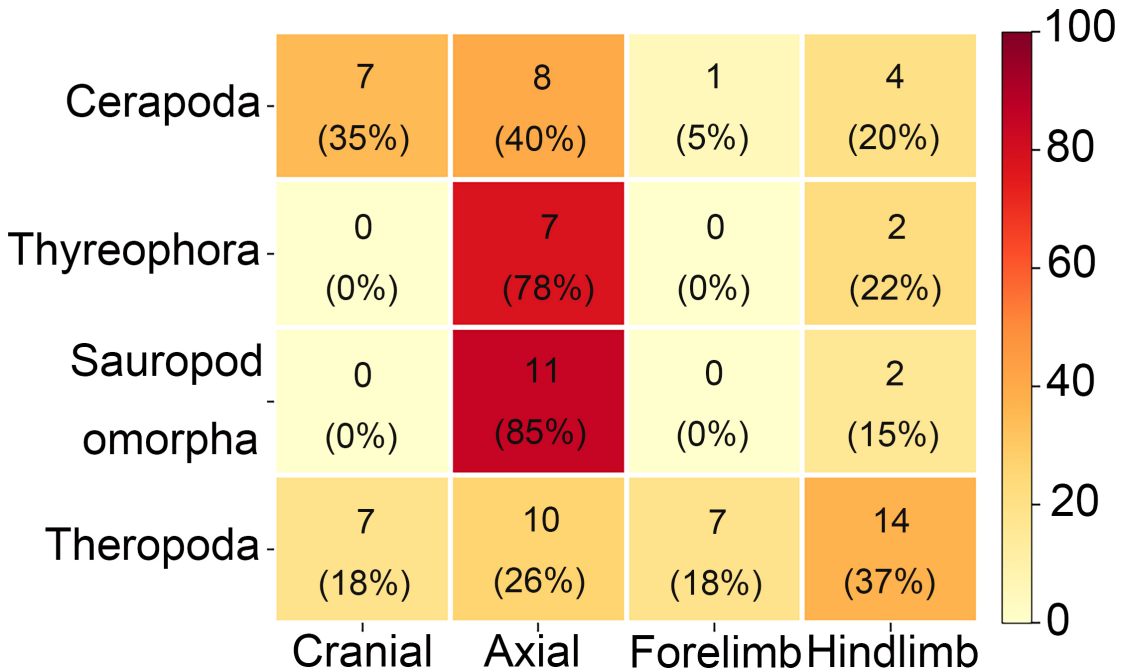


**Figure 5.** Heatmap showing the anatomical distribution of infectious lesions by clade across 81 reported cases of dinosaurian infection. Cell values indicate lesion counts, and shading represents within-clade proportions. Cranial includes the skull and mandible; axial includes vertebrae, ribs, and osteoderms. One non-skeletal lesion was excluded.

## Acknowledgments

The authors thank two anonymous reviewers for their constructive comments and helpful suggestions.

## References

Anné J, Garwood RJ, Lowe T, Withers PJ, Manning PL (2015) Interpreting pathologies in extant and extinct archosaurs using micro-CT. PeerJ 3: e1130. https://doi.org/10.7717/peerj.1130

Baiano MA, Cerda IA, Bertozzo F, Pol D (2024) New information on paleopathologies in non-avian theropod dinosaurs: a case study on South American abelisaurids. BMC Ecology and Evolution 24(1): 6. https://doi.org/10.1186/s12862-023-02187-x

Bennett JE, Dolin R, Blaser MJ [Eds] (2019) Mandell, Douglas, and Bennett's Principles and Practice of Infectious Diseases, 9th edn., Vols 1–2. Elsevier, Philadelphia, 4176 pp.

Chiba K, Ryan MJ, Fanti F, Loewen MA, Evans DC (2018) New material and systematic re-evaluation of *Medusaceratops lokii* (Dinosauria, Ceratopsidae) from the Judith River Formation (Campanian, Montana). Journal of Paleontology 92(2): 272–288. https://doi.org/10.1017/jpa.2017.62

Cohen J, Powderly WG, Opal SM [Eds] (2016) Infectious Diseases, 4th edn., Vols 1–2. Elsevier, Philadelphia, 2016 pp.

Cruzado-Caballero P, Lecuona A, Cerda IA, Díaz-Martínez I (2021) Osseous paleopathologies of *Bonapartesaurus rionegrensis* (Ornithopoda, Hadrosauridae) from Allen Formation (Upper Cretaceous) of Patagonia Argentina. Cretaceous Research 124: 104800. https://doi.org/10.1016/j.cretres.2021.104800

de Souza Barbosa FH, da Costa Ribeiro I, da Costa PVLG, Bergqvist LP (2018) Vertebral lesions in a titanosaurian dinosaur from the Lower-Upper Cretaceous of Brazil. Geobios 51(5): 385–389. https://doi.org/10.1016/j.geobios.2018.08.002

Dunfee BL, Sakai O, Spiegel JH, Pistey R (2005) Solitary fibrous tumor of the buccal space. American Journal of Neuroradiology 26(8): 2114–2116.

Eberth DA, Getty MA (2005) Ceratopsian bonebeds: occurrence, origins, and significance. In: Currie PJ, Koppelhus EB (Eds) Dinosaur Provincial Park: A Spectacular Ancient Ecosystem Revealed. Indiana University Press, Bloomington, 501–536.

Ekhtiari S, Chiba K, Popovic S, Crowther R, Wohl G, Wong AKO, Tanke DH, Dufault DM, Geen OD, Parasu N, Crowther MA, Evans DC (2020) First case of osteosarcoma in a dinosaur: a multimodal diagnosis. The Lancet Oncology 21(8): 1021–1022. https://doi.org/10.1016/S1470-2045(20)30171-6

Fechner RE, Mills SE (1993) Tumors of the Bones and Joints. Atlas of Tumor Pathology, 3rd series, fascicle 8. Armed Forces Institute of Pathology, Washington, DC, 300 pp.

Fiorillo AR, Tykoski RS (2023) Paleobiological inferences from paleopathological occurrences in the Arctic ceratopsian *Pachyrhinosaurus perotorum*. The Anatomical Record 306(7): 1697–1711. https://doi.org/10.1002/ar.25104

Foth C, Evers SW, Pabst B, Mateus O, Flisch A, Patthey M, Rauhut OWM (2015) New insights into the lifestyle of *Allosaurus* (Dinosauria: Theropoda) based on another specimen with multiple pathologies. PeerJ 3: e940. https://doi.org/10.7717/peerj.940

Grady JM, Enquist BJ, Dettweiler-Robinson E, Wright NA, Smith FA (2014) Evidence for mesothermy in dinosaurs. Science 344(6189): 1268–1272. https://doi.org/10.1126/science.1253143

Greenspan A, Remagen W (1998) Differential Diagnosis of Tumors and Tumor-like Lesions of Bones and Joints. Lippincott-Raven, Philadelphia, 435 pp.

Hammer Ø, Harper DAT, Ryan PD (2001) PAST: Paleontological Statistics Software Package for Education and Data Analysis. Palaeontologia Electronica 4(1), art. 4: 9 pp.

Hanna RR (2002) Multiple injury and infection in a sub-adult theropod dinosaur *Allosaurus fragilis* with comparisons to allosaur pathology in the Cleveland-Lloyd Dinosaur Quarry collection. Journal of Vertebrate Paleontology 22(1): 76–90. https://doi.org/10.1671/0272-4634(2002)022[0076:MIAIIA]2.0.CO;2

Hedrick BP, Gao C, Tumarkin-Deratzian AR, Shen C, Holloway JL, Zhang F, Hankenson KD, Liu S, Anné J, Dodson P (2016) An injured *Psittacosaurus* (Dinosauria: Ceratopsia) from the Yixian Formation (Liaoning, China): implications for *Psittacosaurus* biology. The Anatomical Record 299(7): 897–906. https://doi.org/10.1002/ar.23363

Herrera-Castillo CM, Moratalla JJ, Belaústegui Z, Marugán-Lobón J, Martín-Abad H, Nebreda SM, López-Archilla AI, Buscalioni AD (2022) A theropod trackway providing evidence of a pathological foot from the exceptional locality of Las Hoyas (upper Barremian, Serranía de Cuenca, Spain). PLOS ONE 17(4): e0264406. https://doi.org/10.1371/journal.pone.0264406

Holmes RB, Ryan MJ (2013) The postcranial skeleton of *Styracosaurus albertensis*. Kirtlandia 58: 5–37.

Holmes RB, Forster CA, Ryan MJ, Shepherd KM (2001) A new species of *Chasmosaurus* (Dinosauria: Ceratopsia) from the Dinosaur Park Formation of southern Alberta. Canadian Journal of Earth Sciences 38(10): 1423–1438. https://doi.org/10.1139/e01-036

Huchzermeyer FW, Cooper JE (2000) Fibriscess, not abscess, resulting from a localised inflammatory response to infection in reptiles and birds. Veterinary Record 147(18): 515–517. https://doi.org/10.1136/vr.147.18.515

Jackson FD, Garrido A, Schmitt JG, Chiappe LM, Dingus L, Loope DB (2004) Abnormal, multilayered titanosaur (Dinosauria: Sauropoda) eggs from *in situ* clutches at the Auca Mahuevo locality, Neuquén Province, Argentina. Journal of Vertebrate Paleontology 24(4): 913–922. https://doi.org/10.1671/0272-4634(2004)024[0913:AMTDSE]2.0.CO;2

Kirkland JI, DeBlieux DD (2010) New basal centrosaurine ceratopsian dinosaurs from the Wahweap Formation (Middle Campanian), Grand Staircase-Escalante National Monument, southern Utah. In: Ryan MJ, Chinnery-Allgeier BJ, Eberth DA (Eds) New Perspectives on Horned Dinosaurs. Indiana University Press, Bloomington, 117–140.

Kong CZ, Cai JH (2021) Surgery, 4th edn. People's Medical Publishing House, Beijing. [In Chinese]

Lew DP, Waldvogel FA (2004) Osteomyelitis. The Lancet 364(9431): 369–379. https://doi.org/10.1016/S0140-6736(04)16727-5

Longrich NR (2013) *Judiceratops tigris*, a new horned dinosaur from the middle Campanian Judith River Formation of Montana. Bulletin of the Peabody Museum of Natural History 54(1): 51–65. https://doi.org/10.3374/014.054.0103

Lü J, Kobayashi Y, Lee YN, Ji Q (2007) A new *Psittacosaurus* (Dinosauria: Ceratopsia) specimen from the Yixian Formation of western Liaoning, China: the first pathological psittacosaurid. Cretaceous Research 28(2): 272–276. https://doi.org/10.1016/j.cretres.2006.08.005

Meyer KA, Bancroft LW, Dietrich TJ, Kransdorf MJ, Peterson JJ (2011) Imaging characteristics of benign, malignant and infectious jaw lesions: a pictorial review. American Journal of Roentgenology 197(3): W412–W421. https://doi.org/10.2214/AJR.10.7225

Murphy K, Weaver C (2016) Janeway's Immunobiology, 9th edn. Garland Science, New York, 924 pp.

Nabavizadeh A (2023) How *Triceratops* got its face: an update on the functional evolution of the ceratopsian head. The Anatomical Record 306(7): 1951–1968. https://doi.org/10.1002/ar.25196

Nielsen GP, Rosenberg AE (2017) Diagnostic Pathology: Bone, 2nd edn. Elsevier, Philadelphia, 500 pp.

Padian K, Horner JR (2011) The evolution of 'bizarre structures' in dinosaurs: biomechanics, sexual selection, social selection or species recognition? Journal of Zoology 283(1): 3–17. https://doi.org/10.1111/j.1469-7998.2010.00719.x

Persons WS, Currie PJ (2011) The tail of *Tyrannosaurus*: reassessing the size and locomotive importance of the *M. caudofemoralis* in non-avian theropods. The Anatomical Record 294(1): 119–131. https://doi.org/10.1002/ar.21290

Resnick D (2002) Diagnosis of Bone and Joint Disorders, 4th edn., Vols 1–5. W.B. Saunders, Philadelphia, 4944 pp.

Rothschild BM (1988) Stress fracture in a ceratopsian phalanx. Journal of Paleontology 62(2): 302–303. https://doi.org/10.1017/S0022336000029954

Rothschild BM, Tanke DH (1992) Paleoscene 13: paleopathology of vertebrates: insights to lifestyle and health in the geological record. Geoscience Canada 19(2): 73–82.

Rothschild BM, Molnar RE (2005) Sauropod stress fractures as clues to activity. In: Tidwell V, Carpenter K (Eds) Thunder-Lizards: The Sauropodomorph Dinosaurs. Indiana University Press, Bloomington, 381–391.

Rothschild BM, Tanke DH (2005) Theropod paleopathology: state-of-the-art review. In: Carpenter K (Ed) The Carnivorous Dinosaurs. Indiana University Press, Bloomington, 351–365.

Rothschild BM, DePalma R (2013) Skin pathology in the Cretaceous: evidence for probable failed predation in a dinosaur. Cretaceous Research 42: 44–47. https://doi.org/10.1016/j.cretres.2013.01.005

Rothschild BM, Tanke DH, Ford TL (2001) Theropod stress fractures and tendon avulsions as a clue to activity. In: Tanke DH, Carpenter K (Eds) Mesozoic Vertebrate Life. Indiana University Press, Bloomington, 331–336.

Rothschild BM, Surmik D, Bertozzo F (2023) Modern Paleopathology, The Study of Diagnostic Approach to Ancient Diseases, their Pathology and Epidemiology: Let there be light, the light of science and critical thinking. Springer, Cham, 851 pp. https://doi.org/10.1007/978-3-031-28624-7

Ryan MJ (2007) A new basal centrosaurine ceratopsid from the Oldman Formation, southeastern Alberta. Journal of Paleontology 81(2): 376–396. https://doi.org/10.1666/0022-3360(2007)81[376:ANBCCF]2.0.CO;2

Ryan MJ, Russell AP, Eberth DA, Currie PJ (2001) The taphonomy of a *Centrosaurus* (Ornithischia: Ceratopsidae) bonebed from the Dinosaur Park Formation (Upper Campanian), Alberta, Canada, with comments on cranial ontogeny. PALAIOS 16(5): 482–506. https://doi.org/10.1669/0883-1351(2001)016<0482:TTOACO>2.0.CO;2

Ryan MJ, Russell AP, Hartman S (2010) A new chasmosaurine ceratopsid from the Judith River Formation, Montana. In: Ryan MJ, Chinnery-Allgeier BJ, Eberth DA (Eds) New Perspectives on Horned Dinosaurs. Indiana University Press, Bloomington, 181–188.

Sampson SD, Loewen MA, Farke AA, Roberts EM, Forster CA, Smith JA, Titus AL (2010) New horned dinosaurs from Utah provide evidence for intracontinental dinosaur endemism. PLOS ONE 5(9): e12292. https://doi.org/10.1371/journal.pone.0012292

Siviero BCT, Rega E, Hayes WK, Cooper AM, Brand LR, Chadwick AV (2020) Skeletal trauma with implications for intratail mobility in *Edmontosaurus annectens* from a monodominant bonebed, Lance Formation (Maastrichtian), Wyoming, USA. PALAIOS 35(4): 201–214. https://doi.org/10.2110/palo.2019.079

Tanke DH, Rothschild BM (2002) Dinosores: an annotated bibliography of dinosaur paleopathology and related topics—1838–2001. New Mexico Museum of Natural History and Science Bulletin 20: 1–96.

Tanke DH, Farke AA (2006) Bone resorption, bone lesions, and extracranial fenestrae in ceratopsid dinosaurs: a preliminary assessment. In: Carpenter K (Ed) Horns and Beaks: Ceratopsian and Ornithopod Dinosaurs. Indiana University Press, Bloomington, 319–347.

Tanke DH, Rothschild BM (2010) Paleopathologies in Albertan ceratopsids and their behavioral significance. In: Ryan MJ, Chinnery-Allgeier BJ, Eberth DA (Eds) New Perspectives on Horned Dinosaurs. Indiana University Press, Bloomington, 355–384.

Vice RM (2020) The Forelimb and Pectoral Girdle of *Pachyrhinosaurus lakustai* (Ceratopsia, Centrosaurinae). MSc Thesis, University of Alberta, Edmonton, 173 pp.

Wang BY, Eisler J, Springfield D, Klein MJ (2003) Intraosseous epidermoid inclusion cyst in a great toe: a case report and review of the literature. Archives of Pathology & Laboratory Medicine 127(7): e298–e300. https://doi.org/10.5858/2003-127-e298-IEICIA

Witzmann F, Claeson KM, Hampe O, Wieder F, Hilger A, Manke I, Niederhagen M, Rothschild BM, Asbach P (2011) Paget disease of bone in a Jurassic dinosaur. Current Biology 21(17): R647–R648. https://doi.org/10.1016/j.cub.2011.08.006

Xing LD, Dong H, Peng GZ, Shu CK, Hu XD, Jiang H (2009) A scapular fracture in *Yangchuanosaurus hepingensis* (Dinosauria: Theropoda). Geological Bulletin of China 28(10): 1390–1395. https://doi.org/10.12097/gbc.20091004

Xing LD, Bell PR, Rothschild BM, Ran H, Zhang J, Dong Z, Zhang W, Currie PJ (2013) Tooth loss and alveolar remodeling in *Sinosaurus triassicus* (Dinosauria: Theropoda) from the Lower Jurassic strata of the Lufeng Basin, China. Chinese Science Bulletin 58(16): 1931–1935. https://doi.org/10.1007/s11434-013-5765-7

Xing LD, Rothschild BM, Ran H, Miyashita T, Persons WS IV, Sekiya T, Zhang J, Wang T, Dong Z (2015) Vertebral fusion in two Early Jurassic sauropodomorph dinosaurs from the Lufeng Formation of Yunnan, China. Acta Palaeontologica Polonica 60(3): 643–649. https://doi.org/10.4202/app.00001.2013

Xing LD, Rothschild BM, Randolph-Quinney PS, Wang Y, Parkinson AH, Ran H (2018) Possible bite-induced abscess and osteomyelitis in *Lufengosaurus* (Dinosauria: Sauropodomorpha) from the Lower Jurassic of the Yimen Basin, China. Scientific Reports 8(1): 5045. https://doi.org/10.1038/s41598-018-23451-x

Xing LD, Rothschild BM, Du C, Wang D, Wen K, Su J (2024) New palaeopathology cases of *Allosaurus fragilis* (Dinosauria: Theropoda). Historical Biology 36(1): 203–208. https://doi.org/10.1080/08912963.2022.2155817

## Additional information

### Conflict of interest

The authors have declared that no competing interests exist.

### Ethical statement

No ethical statement was reported.

### Artificial Intelligence (AI) use

The authors accept full responsibility for the content of the manuscript, including the disclosure of any use of AI.
Regarding the use of AI in the preparation of this manuscript, the authors declare the following: Claude.
**Used for:** Other.
The authors used AI for references checking and manuscript proofreading.

### Funding

This research was funded by the 2025 Heilongjiang Provincial Natural Science Foundation Youth Project Type C (JJ2025QC0704), the National Natural Science Foundation of China (No. 42488201), the "Deep-time Digital Earth" Science and Technology Leading Talents Team Funds for the Central Universities for the Frontiers Science Center for Deep-time Digital Earth, China University of Geosciences (Beijing) (Fundamental Research Funds for the Central Universities; grant number: 2652023001), the 111 Project (B20011), and the Fundamental Research Funds for the Central Universities (265QZ201903).

### Author contributions

Donghao Wang conducted the specimen description and diagnosis, collected and analysed the data, and drafted the manuscript. Lida Xing contributed to the specimen description, diagnosis, and manuscript preparation. Bruce M. Rothschild contributed to the diagnosis, data collection, and manuscript preparation. Chunlei Du, Kexiang Wen, Jin Lin, and Mengling Kang carried out specimen photography, CT scanning, and structured-light scanning. Jiayin Su contributed to the diagnosis. All authors reviewed and approved the final version of the manuscript.

### Author ORCIDs

L. Xing https://orcid.org/0000-0003-3923-9206
B.M. Rothschild https://orcid.org/0000-0003-1327-6615

### Data availability

The Supplementary material is available at https://doi.org/10.6084/m9.figshare.31850866.

# Supplementary material 1

## Supplementary information

Authors: Donghao Wang, Lida Xing, Bruce M. Rothschild, Chunlei Du, Kexiang Wen, Jin Lin, Mengling Kang, Jiayin Su
Data type: xlsx
Copyright notice: This dataset is made available under the Open Database License (http://opendatacommons.org/licenses/odbl/1.0). The Open Database License (ODbL) is a license agreement intended to allow users to freely share, modify, and use this Dataset while maintaining this same freedom for others, provided that the original source and author(s) are credited.
Link: https://doi.org/10.3897/fr.29.193112.suppl1